Integrative transcriptomic profiling of a mouse model of hypertension-accelerated diabetic kidney disease

Frederikke E. Sembach[1,2], Helene M. Ægidius[1], Lisbeth N. Fink[1], Thomas Secher[1], Annemarie Aarup[1], Jacob Jelsing[1], Niels Vrang[1], Bo Feldt-Rasmussen[2,3], Kristoffer T. G. Rigbolt[1], Jens C. Nielsen[1], Mette V. Østergaard*[1]

[1]Gubra ApS, Hørsholm Kongevej 11B, 2970 Hørsholm, Denmark

[2]Department of Clinical Medicine, University of Copenhagen, Blegdamsvej 3B, 2200 Copenhagen, Denmark

[3]Department of Nephrology, Rigshospitalet, University of Copenhagen, Denmark.

*Corresponding author: Mette V. Østergaard; mvo@gubra.dk; +45 31 52 26 50

KEY WORDS

Diabetic kidney disease, mouse model, laser-capture microdissection, single-nucleus, glomerulus, RNA sequencing

SUMMARY STATEMENT

Combining single-nucleus RNA sequencing with glomerular and cortical gene expression profiling can link kidney transcriptome signatures to specific cell types in an advanced mouse model of hypertension-accelerated diabetic kidney disease.

ABSTRACT

The current understanding of molecular mechanisms driving diabetic kidney disease (DKD) is limited, partly due to the complex structure of the kidney. To identify genes and signalling pathways involved in the progression of DKD, we compared kidney cortical vs. glomerular transcriptome profiles in

uninephrectomized (UNx) db/db mouse models of early-stage (UNx only) and advanced (UNx plus AAV-mediated renin overexpression, UNx-Renin) DKD using RNA sequencing (RNAseq). Compared to normoglycemic db/m mice, db/db UNx and db/db UNx-Renin mice showed marked changes in kidney cortical and glomerular gene expression profiles. UNx-Renin mice displayed more marked perturbations in gene components associated with activation of the immune system and enhanced extracellular matrix remodelling, supporting histological hallmarks of progressive DKD in this model. Single-nucleus RNAseq enabled linking transcriptome profiles to specific kidney cell types. In conclusion, integration of RNAseq at the cortical, glomerular and single-nucleus level provides enhanced resolution of molecular signalling pathways associated with disease progression in preclinical models of DKD, and may thus be advantageous for identifying novel therapeutic targets in DKD.

INTRODUCTION

Diabetic kidney disease (DKD) is a microvascular complication of diabetes and the most common cause of chronic kidney disease worldwide, accounting for approximately 50% and 25% of patients with kidney failure in the USA and EU, respectively (United States Renal Data System, 2018; Kramer *et al.*, 2019). DKD is characterized by progressive loss of kidney function as defined by a decline in glomerular filtration rate and proteinuria due to impairment of the glomerular filtration barrier. In addition, patients with DKD demonstrate kidney histopathological alterations including glomerular hypertrophy, glomerulosclerosis, tubulointerstitial inflammation and fibrosis (Fioretto and Mauer, 2007; Tervaert *et al.*, 2010).

Despite drug therapeutic advances in hyperglycemia and hypertension management (Lewis *et al.*, 1993; Brenner *et al.*, 2001; Wanner *et al.*, 2016; Mann *et al.*, 2017; Perkovic *et al.*, 2019; Heerspink *et al.*, 2020), the combination of increased diabetes prevalence and life expectancy in diabetes patients have led to an increase in patients with DKD progressing to kidney failure (McCullough *et al.*, 2019). Hence, prevention and treatment of DKD has become a healthcare priority. The unmet clinical need is partly due to lack of animal models that closely mimic the molecular mechanisms associated with late-stage DKD. Hypertension, a common comorbidity in diabetes and a driving factor of DKD progression, is absent in most rodent models commonly used in preclinical DKD research, including the uninephrectomized (UNx) *db/db* mouse model of early-stage DKD (Levine, Iacovitti and Robertson, 2008). Induction of persistent hypertension by adeno-associated virus delivery of renin (ReninAAV) has recently been reported to accelerate kidney injury in *db/db* UNx mice (Harlan, Heinz-Taheny, Sullivan, *et al.*, 2018). Accordingly, the *db/db* UNx-Renin mouse

presents with hallmarks of late-stage DKD including markedly increased urine albumin-to-creatinine ratio (ACR), advanced glomerulosclerosis, and elevated serum creatinine levels.

Because the glomerulus has long been considered the primary site of injury in DKD, understanding transcriptome changes in the glomerulus is key from a drug discovery perspective. These investigations are challenged by the fact that glomeruli constitute only a small proportion of renal cortical cells and bulk RNAseq does not capture glomerulus-specific gene expression changes. Therefore, gene expression analysis applied to glomeruli isolated by laser-capture microdissection (LCM) improves resolution of glomerular transcriptome changes associated with DKD progression (Woroniecka *et al.*, 2011; Levin *et al.*, 2020). This work flow has been applied in drug discovery projects for other metabolic diseases such as obesity (Paulsen *et al.*, 2009; Zhang *et al.*, 2019).

Although recent developments in transcriptomics enable analysis at the single-cell or single-nucleus level to identify and characterize cell types, these techniques have a low gene detection per cell and a high cost, resulting in limited sensitivity to identify DEGs at low expression level (Conesa *et al.*, 2016; Wang *et al.*, 2019). Therefore, an integrative approach leveraging the cell-level resolution of snRNAseq with the sensitivity of RNAseq has proven to be instrumental for gaining detailed insight into the underlying molecular mechanisms involved in specific cell types (Barwinska *et al.*, 2021; Sokolowski *et al.*, 2021).

The current study investigated kidney pathology and disease-related gene and pathway regulations in kidney cortex and glomeruli in mouse models of early-stage (UNx) and advanced (UNx-Renin) DKD. Using a multi-transcriptomic approach, we integrated bulk transcriptomic profiling of kidney cortex and glomeruli with snRNAseq to improve the resolution of cell-specific transcriptomic changes.

RESULTS

Diabetic mouse models of early-stage (UNx) and advanced (UNx-Renin) DKD.

ReninAAV administration was evaluated for renal effects and transcriptome changes in the diabetic UNx mouse model of DKD, while UNx mice injected with LacZAAV and healthy db/m mice served as controls (Fig. 1A-B). UNx and UNx-Renin mice demonstrated significantly higher degree of obesity and hyperglycaemia as compared to lean db/m controls (both $P<0.001$, Fig. 2A-B). Whereas UNx and UNx-Renin mice showed similar levels in systolic arterial blood pressure at study week 4 (UNx, 137.5 ± 0.9 mmHG; UNx-Renin, 140.9 ± 1.0 mmHg), ReninAAV induced hypertension in UNx *db/db* mice from study week 4 to 10 (+18.8 mmHg, *data not shown*). Urine ACR was significantly increased in

UNx mice at study weeks 6 and 12 when compared to db/m controls (both P<0.001), and was further augmented in UNx-Renin mice (both time points P<0.001, Fig. 2C). Kidney weight was increased in UNx and UNx-Renin mice compared with db/m controls (both P<0.001, Fig. 2D). Glomerular hypertrophy was evident in both UNx and UNx-Renin mice (Fig. 2E). Quantification of total glomerular PAS mass indicated increased glomerulosclerosis in UNx and UNx-Renin mice compared to db/m controls (both P<0.001), being most advanced in UNx-Renin mice (p<0.001 vs. UNx, Fig. 2F). To summarize, measurements indicate that a single injection with ReninAAV exacerbates kidney injury, notably albuminuria and glomerulosclerosis, in UNx-renin mice compared with UNx mice, but does not affect body weight or blood glucose levels.

To study gene expression changes accelerated by UNx and ReninAAV administration in diabetic mice, RNAseq was performed on kidney cortex samples and laser-capture microdissected (LCM) glomeruli from db/m, UNx and UNx-Renin mice. Comparison of gene expression changes between UNx (early-stage DKD) and UNx-Renin (advanced stage DKD) mice are presented in Supplementary Figure 1. 3,039 genes were differentially expressed between UNx and UNx-Renin mice in kidney cortex, while 770 genes were differentially expressed in glomeruli between the same groups (Supplementary Figure 1). Gene set analysis using the Reactome pathway database (Fabregat *et al.*, 2018) identified the *Immune System* as the most significantly affected in the kidney cortex of UNx-Renin mice compared to UNx mice, while *Extracellular Matrix (ECM) Organization* was most affected in glomeruli (Supplementary Figure 1).

Highly specific gene expression profiles in glomeruli versus kidney cortex.

To characterize glomerular-specific gene expression changes in the UNx and UNx-Renin mouse models of DKD, we compared the glomerular transcriptome with the full kidney cortex transcriptome. First, we performed a principal component analysis (PCA), which is a dimensionality reduction method used to assess the similarity of the gene expression profiles from individual samples, with samples closest to each other being most similar. The PCA demonstrated a clear separation between the glomerular transcriptome signature and kidney cortex from db/m, UNx and UNx-Renin mice (Fig. 3A). The difference between isolated glomeruli and kidney cortex samples explained the majority of variance in the data set as indicated in percent (94 %, PC1), followed by the difference between phenotypes (db/m, UNx, UNx-Renin, 2%, PC2, Fig. 3A). Gene expression analysis of UNx and UNx-Renin mice compared to healthy db/m controls, revealed a higher number of DEGs in the kidney cortex of UNx mice (5,500 DEGs) than in UNx-Renin mice (4,470 DEGs, Fig. 3B). The opposite was seen for the glomerular transcriptome (UNx, 3,049 DEGs; UNx-Renin, 4,164 DEGS;

Fig. 3B). Interestingly, few DEGs overlapped between kidney cortex and isolated glomeruli for both UNx (1,472 DEGs) and UNx-Renin (1,590 DEGs) mice compared to healthy db/m controls (Fig. 3C). Overall, these data substantiate that RNAseq of kidney cortex does not specifically reflect glomerular gene expression changes in both the UNx and UNx-Renin models of DKD and highlights the importance of profiling the transcriptome of kidney structures separately.

A gene set enrichment analysis was performed to assess changes in signalling pathways specific to the UNx and UNx-Renin groups, respectively, including both up- and downregulated genes in the signalling pathways (Fig. 3D, Supplementary Figure 2). Compared to db/m controls, *Metabolism* was the most regulated pathway in the kidney cortex of UNx mice, predominantly driven by increased expression of *Rbp2*, *Cyp2d9* and *Ugt1a10* (Supplementary Table 1). In contrast, changes in cortical gene signatures of UNx-Renin mice were associated with the *Immune System*, including both the innate immune system (*Neutrophil degranulation, Toll-like Receptor Cascades)* and cytokine signalling (*Signalling by Interleukins, TNFR2 non-canonical NF-kB pathway*, Supplementary Figure 2). Concordantly, increased expression of chemokines (*Cxcl1, Cxcl2*), vascular cell adhesion molecule (*Vcam1*), toll-like receptor (*Tlr4*) and complement component genes (*C3, C6, C7*) were observed in UNx-Renin mice. Glomerular gene expression signatures in UNx and UNx-Renin mice were mainly associated with *ECM Organization* (Fig. 3D) as exemplified by increased expression of several genes involved in fibrogenesis (e.g. *Col5a1, Col5a3, Fn1, Lox, Mmp3, Mmp8, Mmp12, Adamts4, Serpine 1 and Timp1,* Supplementary Table 2). Consistent with marked glomerulosclerosis in UNx-Renin mice, ECM-associated gene expression changes were more pronounced in UNx-Renin mice, where additional markers of fibrogenesis were significantly upregulated including *Col1a1, Col3a1, Col6a1, Col6a2*, *and Mmp7.*

Single-nucleus RNA sequencing reveal glomerular cell-specific regulations in DKD pathogenesis.

To further investigate the marked transcriptomic changes between normoglycemic db/m controls and diabetic, hypertensive UNx-Renin mice, we performed snRNAseq to associate gene expression changes to specific cell types harvested from the kidney cortex. Unsupervised clustering identified 21 cell clusters. Based on canonical cell-type markers each cluster were assigned to distinct cell types. Figure 4A shows the projection of single nuclei onto two-dimensional Uniform Manifold Approximation and Projection (UMAP) space coloured by assigned cell types. In addition to all major cortical cell types such as podocytes, mesangial cells, endothelial cells, macrophages, proximal tubule cells, distal tubule cells and collecting duct cells, we detected specific gene signatures of Loop of Henle-associated cell types, indicating the presence of medullary cells in the samples. Our

preliminary analysis suggested reduced podocyte and endothelial cell proportions in UNx-Renin mice (Figure 4B) compared to db/m control.

The combination of snRNAseq data with kidney cortex and LCM isolated glomeruli based RNAseq data allowed us to associate DEGs to specific cell types in UNx-Renin mice (Fig. 4C). We found that a large proportion of cortical DEGs in UNx-Renin mice were linked to cells in the S3 segment of the proximal tubule. In contrast, glomerular DEGs identified were distributed more broadly including podocytes, mesangial cells, macrophages, and endothelial cells. Furthermore, we superimposed DEGs found between UNx mice and db/m controls, or between UNx-Renin and UNx mice to specific cell types in Supplementary Figure 3. Consistent with gene expression changes in the *Immune System* pathway in the kidney cortex between UNx-Renin and UNx mice (Supplementary Figure 1), cortical DEGs identified between the two models were linked to macrophages. Finally, a gene set analysis was applied to characterize changes in signalling pathways associated with podocyte, endothelial cell and mesangial cell populations in UNx and UNx-Renin mice (Supplementary Figure 4-6). Key genes driving pathway changes are presented in Figure 5.

In UNx-Renin mice, podocyte markers were downregulated in the kidney cortex (*Nphs1*, $P<0.01$ compared to db/m controls), and glomeruli (*Nphs1* and *Nphs2,* compared to both $P<0.001$ vs. db/m; $P<0.001$ and $P<0.01$ vs. UNx, Fig. 5A), indicating podocyte loss. Compared to db/m controls, both UNx and UNx-Renin mice showed downregulation of the endothelial cell marker *Mapk12* in the kidney cortex (both $P<0.001$ vs. db/m controls), while *Mapk12* expression was only downregulated in glomeruli of UNx-Renin mice ($P<0.001$ versus db/m, $P<0.05$ vs UNx mice) (Fig. 5B). However, overall our gene set analysis of endothelial cell markers showed more pronounced changes in UNx mice than in UNx-Renin mice when compared to db/m controls, suggesting that endothelial cell injury may occur in early stage of DKD (Supplementary Figure 5).

Col5a1, *Col5a3*, *Fn1* and *Mmp14* expression was associated with mesangial cells, supporting increased ECM production in glomeruli. *Col5a3*, *Fn1* and *Mmp14* were upregulated in the kidney cortex and glomeruli of UNx-Renin mice compared to both db/m controls and UNx mice (Figure 5C) underscoring the advanced progression of glomerulosclerosis in this model of late-stage DKD.

DISCUSSION

We report highly different glomerular and cortical transcriptome changes in mouse models of early-stage (UNx) and advanced (UNx-Renin) DKD. The transcriptome signatures identify metabolic and immune responses as essential disease drivers in UNx and UNx-Renin mice, respectively, while

glomerular ECM regulation is seen in both models but most prominent in UNx-Renin mice. This is consistent with the advanced glomerulosclerosis in the model. Our study highlights the utility of combining bulk RNAseq with snRNAseq to define cell type-specific gene regulations important for DKD progression and thus further enabling identification of novel drug targets. Additionally, the gene expression profiling of our two mouse models of DKD allows researchers to select the most appropriate preclinical model for drug testing.

The diabetic *db/db* UNx mouse model of DKD has been well-characterized since the model was first introduced in 1980 (Bower *et al.*, 1980). While the *db/db* UNx mouse presents with mesangial matrix expansion and increased albuminuria, the model does not capture the decline in glomerular filtration rate as often seen in patients with advanced DKD (Bower *et al.*, 1980; Ninichuk, Kulkarni, Clauss and H. J. Anders, 2007; Levine, Iacovitti and Robertson, 2008; Sembach *et al.*, 2019). The lack of decline in glomerular filtration rate may be caused by the absence of hypertension in the model (Levine, Iacovitti and Robertson, 2008), which is a common comorbidity in DKD (Long and Dagogo-JAck, 2011). The UNx-Renin mouse represents a promising model of progressive DKD (Harlan, Heinz-Taheny, Sullivan, *et al.*, 2018). Accordingly, ReninAAV administration induces persistent hypertension and has recently been shown to accelerate DKD progression in diabetic UNx mice (Harlan, Heinz-Taheny, Sullivan, *et al.*, 2018; Østergaard *et al.*, 2021). Our study corroborates previous findings in the UNx-Renin model, demonstrating biochemical and histological features of progressive DKD, notably severe albuminuria and advanced glomerulosclerosis (Harlan, Heinz-Taheny, Overstreet, *et al.*, 2018; Harlan, Heinz-Taheny, Sullivan, *et al.*, 2018; Østergaard *et al.*, 2021). Although several transcriptomic studies have been reported in the *db/db* UNx and UNx-Renin mouse model, knowledge on disease-associated gene expression changes in these models is based on pre-selected gene sets (Ninichuk, Kulkarni, Clauss and H.-J. Anders, 2007; Harlan, Heinz-Taheny, Overstreet, *et al.*, 2018; Harlan, Heinz-Taheny, Sullivan, *et al.*, 2018). Consequently, global gene expression profiling could help validating the clinical translatability of these models. In this report, we characterize the global kidney transcriptome changes in the UNx and UNx-Renin mouse model using RNAseq.

As expected, RNAseq data revealed a clear separation of cortical versus glomerular transcriptome signatures, reflecting unique transcriptional signatures in glomeruli that were not shared in the kidney cortex as exemplified by the expression of *Nphs1, Nphs2, Col5a3* and *Mmp14*. These genes were significantly regulated in the glomeruli of UNx mice compared to healthy db/m controls but not in the kidney cortex. Because bulk RNAseq analysis captures a composite gene expression signal from the whole tissue, hence from all cell types in the sample, the low number of glomerular cells compared to other kidney cortical cell types cannot be captured by bulk RNAseq.

In the present study, gene expression changes associated with the *Immune System* were prominent in the kidney cortex in diabetic UNx-Renin mice, while diabetic UNx mice demonstrated more robust changes in metabolism-associated genes when compared to healthy db/m controls. This is consistent with previous studies reporting increased interstitial inflammation along with upregulation of inflammatory markers (e.g. *C3, Cxcl2*) in UNx-Renin mice compared to UNx mice (Harlan, Heinz-Taheny, Overstreet, *et al.*, 2018; Harlan, Heinz-Taheny, Sullivan, *et al.*, 2018). Collectively, these findings are in agreement with pronounced kidney immune system responses in patients with advanced DKD as compared to early-stage DKD (Fan *et al.*, 2019). In combination, snRNAseq and bulk RNAseq analysis further emphasized that differences in cortical immune system changes in diabetic UNx-Renin compared to UNx mice were mainly associated with gene markers of macrophage recruitment. Correspondingly, kidney macrophage infiltration has been shown to correlate with impaired kidney function in patients with DKD (Nguyen *et al.*, 2006). We found an increased expression of *Cxcl1* and *Cxcl2,* encoding proinflammatory chemokines that stimulate monocyte infiltration (Pichler *et al.*, 2017), while *C3*, *C6* and *C7* genes are part of the complement system, which is known to be activated in human DKD (Woroniecka *et al.*, 2011; Ju *et al.*, 2013; Sircar *et al.*, 2018; Yiu *et al.*, 2018). Additionally, a negative correlation between C3 upregulation in tubulointerstitium and decreased GFR has previously been shown in patients with DKD (Tang *et al.*, 2020). Upregulation of *Vcam1* in UNx-Renin mice has been reported in other experimental mice models of DKD (KK-Ay, BTBR *ob/ob*) (Omote *et al.*, 2014; Granqvist *et al.*, 2020), and is known to recruit leukocytes to site of inflammation. In agreement, an upregulation of VCAM-1 in tubulointerstitium together with a positive correlation between elevated serum VCAM-1 and albuminuria levels have been reported in DKD patients (Schmid *et al.*, 2006; Wong *et al.*, 2008). Immune responses in UNx-Renin mice were also characterized by upregulation of markers associated with toll-like receptor (TLR) signalling as exemplified by the increased gene expression of *Tlr4* in kidney cortex and glomeruli of UNx-Renin mice compared to healthy db/m controls. Concordantly, gene and protein expression of TLR4 is upregulated in glomeruli and tubulointerstitium of patients with DKD (Verzola *et al.*, 2014). In support of the relevance of TLRs in DKD, inhibition of TLR signalling has been shown to improve albuminuria in mouse models of DKD (Cha *et al.*, 2013; Lin *et al.*, 2013). Overall, our data supports that the *db/db* UNx-Renin mouse model recapitulates human DKD in terms of immune response and indicate inflammatory pathway activation as key to the pathogenesis.

The glomerulus has long been considered the primary site of injury during DKD progression due to changes in the glomerular structure such as mesangial expansion, glomerular basement membrane thickening and glomerulosclerosis (Fioretto and Mauer, 2007; Tervaert *et al.*, 2010; Woroniecka *et*

al., 2011). As molecular drivers of glomerulosclerosis in diabetic UNx and UNx-Renin mice, our glomerular gene expression analysis confirmed upregulation of several fibrogenesis-associated genes (e.g., *Col1a1*, *Col5a1, Col5a3, Fn1, Mmp14*). These results are consistent with prior studies in microdissected glomeruli from patients diagnosed with diabetic nephropathy that showed increased expression of *Col1a1*, *Col5a1* and *Fn1* (Woroniecka *et al.*, 2011; Levin *et al.*, 2020). Especially fibronectin (*Fn1)* has been linked to accumulation of ECM proteins, and treatment with the SGLT2 inhibitor canagliflozin in individuals with T2D and elevated urine ACR, has been shown to downregulate plasma levels of fibronectin, thereby reducing the fibrosis biomarker (Heerspink *et al.*, 2019). Also, the gene expression of Col1a1 is upregulated in human DKD glomeruli (Woroniecka *et al.*, 2011; Ju *et al.*, 2013; Levin *et al.*, 2020). Using snRNAseq analysis, we found that most DEGs involved in fibrogenesis were associated with mesangial cells, confirming that mesangial cells are critical players in DKD progression and may be potential targets for prevention and treatment of glomerulosclerosis. In UNx-Renin mice, we identified nephrin family-interactions as being the top-regulated pathway in podocytes, primarily associated with downregulation of the key podocyte markers, *Nphs1* and *Nphs2*. Downregulation of these genes is consistent with podocyte loss observed in *db/db* mice (Susztak *et al.*, 2006). *NPHS1* and *NPHS2* together with several other podocytes-specific genes are also downregulated in human DKD studies (Woroniecka *et al.*, 2011), emphasizing the role podocyte injury plays in DKD pathogenesis. Our analysis demonstrates higher expression levels of podocyte-specific genes in glomeruli compared to the kidney cortex, highlighting the advantage of isolating glomeruli for gaining further insight into gene expression changes associated with specific glomerular cell types.

In contrast, we found that several endothelial cell-specific genes were regulated in the kidney cortex of UNx mice compared to db/m controls, whereas the same was not seen for UNx-Renin mice, suggesting that changes in the microvasculature occurs during early stages of DKD. Similarly, features of endothelial dysfunction and changes in angiogenesis have been observed in patients with early DKD (Jensen *et al.*, 1989; Wilson *et al.*, 2019).

Limitations in the study should be considered. First, snRNAseq analysis was limited by the small sample size. We therefore integrated the specificity of snRNAseq with the sensitivity of bulk RNAseq to assign gene expression changes to individual kidney cell types. A similar approach has recently been used for bulk RNAseq to quantitively characterize transcriptomic profiles with single-cell resolution (Ægidius *et al.*, 2020; Dong *et al.*, 2021) or to infer cell type proportions by bulk RNAseq deconvolution (Fan *et al.*, 2019). In our study, we captured all major cell types in the kidney except for glomerular endothelial cells, which have been observed in previous studies (Fu *et al.*, 2019; Jourde-Chiche *et al.*, 2019). The lack of glomerular endothelial cell gene expression signatures might

be due to bias towards specific cell types during nuclei isolation, or the resolution of the clusters used for the bioinformatical analysis. Therefore, further sub-analysis of the endothelial cell population would be needed to confirm whether glomerular endothelial cells are captured. Combining bulk RNAseq with snRNAseq constitutes a powerful tool to detect cell-specific changes. Notably, it provided us with cell type specific DEGs and specific pathway regulations in glomerular cell types (e.g., podocytes, mesangial cells, endothelial cells).

CONCLUSION

The present study allowed for detection of gene expression changes specific to glomeruli using LCM of kidney cortical samples. The transcriptomic changes identified in the *db/db* UNx-Renin mouse model supports histological hallmarks of progressive DKD in this model. Combining snRNAseq with RNAseq of glomeruli and kidney cortex, enables further resolution of the transcriptome signatures with respect to kidney cell types. Using this approach, the integration of different RNAseq methods has the potential to improve future drug discovery activities including selection of appropriate preclinical mouse model of DKD.

MATERIALS AND METHODS

Animals

The Danish Animal Experiments Inspectorate approved all experiments which were conducted using internationally accepted principles for the use of laboratory animals (2018-15-0201-01533). Female C57BLKS *db/db* (BKS.Cg-Dock7^{m}+/+Lepr^{db}J) and db/m mice (Dock7m +/+ Leprdb) (Charles River Laboratories, Italy) arrived two to three weeks prior to surgery and were housed in a controlled environment (12 h light/dark cycle, 21 ± 2 °C, humidity 50 ± 10%). Each animal was identified by an implantable subcutaneous microchip (PetID Microchip, E-vet, Haderslev, Denmark). Uninephrectomy was performed in 8-week-old *db/db* mice as described in detail previously (Sembach *et al.*, 2019), however, in this study we removed the right kidney instead of the left kidney. Age-matched unoperated db/m mice served as healthy controls. The *db/db* UNx mice were randomized based on body weight and blood glucose levels, and received either a single injection of 1*10^{10} genome copies (GC) LacZAAV (UNx), which served as a negative control, or 2*10^{10} GC ReninAAV (UNx-Renin) at 12 weeks of age (Vector Biolabs, Malvern, PA)(Harlan, Heinz-Taheny, Sullivan, *et al.*, 2018). Mice had ad libitum access to tap water and chow (3.22 kcal/g, Altromin 1324, Brogaarden, Hoersholm, Denmark). Animals were terminated by cardiac puncture under isoflurane anesthesia 12 weeks after

injection of viral vector. After dissection, the kidney was cut sagitally and the two halves collected for histopathological evaluation and RNAseq, respectively.

Blood pressure

At study week 4 and 10, systolic arterial blood pressure was measured using tail cuff plethysmography by a mouse tail cuff system (IITC Life Science, Woodland Hills, CA). Animals (n = 5-6) were randomly selected for blood pressure measurement and acclimated to the system for 4 consecutive days prior to the actual data acquisition on day 5.

Blood and Urine Analyses

Blood glucose was measured throughout the study by collecting blood from the tail vein of nonfasted mice into heparinized glass capillary tubes and immediately suspending in glucose/lactate system solution buffer (EKF Diagnostics, Barleben, Germany). Blood glucose was measured using a BIOSEN c-Line glucose meter (EKF Diagnostics) according to the manufacturer's instructions. Spot urine samples were collected 6 and 12 weeks after injection of viral vector directly from the vulva to determine the urine albumin-to-creatinine ratio (ACR). Urine creatinine was measured using the CREP2 kit (Roche Diagnostics, Mannheim, Germany) on a Cobas C-501 autoanalyzer. Urine albumin was measured using a Mouse Albumin ELISA Kit (Bethyl Laboratories, Montgomery, TX, US).

Histopathology

Kidney samples were fixated for 24 hours in a 3.3% glyoxal solution (Sigma-Aldrich, Denmark) at 4°C. Samples were embedded in blocks of paraffin and 3 µm kidney sections were cut on a microtome. Periodic acid–Schiff (PAS) staining was performed using standard procedures. Briefly, kidney sections were deparaffinized and oxidized in 0.5% periodic acid (Sigma-Aldrich, Denmark). Next, sections were incubated with Schiff's reagent (Sigma-Aldrich, Denmark) and counterstained with Mayer's hematoxylin (Dako, Denmark). Sections were dehydrated and mounted with Pertex (Histolab, Sweden). PAS stained slides were scanned in a Scanscope AT slide scanner (Leica, Denmark) under a 20x objective.

Total glomerular PAS positive staining was determined by AI-assisted image analysis using VIS software package (version 2020.01.3, Visiopharm, Denmark). Scanned slides were analysed using a two-step protocol. Firstly, all glomeruli were detected using a trained U-NET network architecture. Next, PAS positive surface area of the glomerular tuft was segmented using a simple threshold after

PAS colour deconvolution. Total PAS mass was expressed as total mass (mg) of positive staining by multiplying the glomerular PAS positive fractional area (%) with the terminal kidney weight.

Laser Capture Microdissection

Frozen kidneys were sectioned on a cryostat (CM3050 S, Leica, Germany) into 20 µm thick sections and collected on PEN membrane glass slides (LCM0522, ThermoFisher, Waltham, MA, USA) for LCM. Tissue-mounted slides were stored at -80 °C until further processing.

Prior to LCM, sections were thawed for 5 min at 4 °C and then dipped in cold 70% ethanol to remove any remaining OCT (TissueTek O.C.T., Sakura Finetek, Denmark) from the cryosectioning. The sections were stained for 5 min in a 0.1% cresyl violet acetate (Sigma-Aldrich, Søborg, Denmark) solution dissolved in 70% ethanol. After staining, sections were dehydrated in 96% and two times 100% ethanol for 30 seconds each at 4 °C and finally allowed to dry in fume hood for 2 min at room temperature. LCM was then performed with the Arcturus® Veritas™ LCM equipment (Life Technologies, Carlsbad, CA, USA). The glomeruli were identified under microscope and captured by a combination of infrared (IR) laser capturing and ultraviolet (UV) laser cutting. The glomeruli were captured on CapSure® Macro LCM Caps (LCM0211, ThermoFisher, Waltham, MA, USA). A total of 200 glomeruli were isolated per animal sample. The CapSure® Macro LCM cap with captured tissue was inserted on to a 0.5 mL Eppendorf tube (022431005, Eppendorf, Germany) with 50 µL of Extraction buffer (Arcturus® PicoPure® RNA Isolation Kit, KIT0204, ThermoFisher, Waltham, MA, USA). The tube was inverted to make sure the tissue was covered by the extraction buffer. The tube with the LCM cap was incubated for 30 min at 42 °C to ensure sufficient lysis. After lysis, the lysate was spun down, the LCM cap was removed, and the tube was stored at -80 °C until RNA purification.

RNA purification of LCM samples

RNA extraction was performed using the Arcturus® PicoPure® RNA Isolation Kit (KIT0204, ThermoFisher, Waltham, MA, USA), following the protocol recommended by manufacturer. Samples were treated with DNase for 10 minutes (AM1906, ThermoFisher, Waltham, MA, USA) before adding stop solution. RNA was purified over two rounds using a total of 20 µL of RNase free water. RNA quantity was determined using NanoDrop (NanoDrop 2000/2000c, ThermoFisher, Waltham, MA, USA) as recommended by the manufacturer. RNA quality was determined using an Agilent Bioanalyzer with RNA 6000 Pico Kit (5067-1513, Agilent, Santa Clara, CA, USA) as recommended by the manufacturer. The RNA samples were then stored at -80^{o}C until further processing.

RNA purification of kidney cortex samples

RNA from snap-frozen kidney cortex samples (~15 mg per animal) stored at −80°C was extracted using the NucleoSpin® 8 RNA kit (Macherey-Nagel) and a vacuum manifold. The RNA quantity was measured using NanoDrop, and RNA quality determined using an Agilent Bioanalyzer with RNA 6000 Nano Kit (5067-1511, Agilent, Santa Clara, CA, USA).

Library preparation and sequencing of kidney cortex and LCM samples

cDNA library preparation was performed using NEBNext ® Ultra™ II Directional RNA Library Prep Kit for Illumina® (E7760L, NEG, Ipswich, MA, USA). The number of cycles used for cDNA amplification was 16 for kidney cortex samples and 18 for LCM samples. The sequencing of cDNA libraries was performed with NS® 500 high Output Kit v2 (75 cycles) (Illumina, San Diego, CA, USA) on an Illumina NextSeq 500 platform (Illumina, San Diego, CA, USA). The gene expression level is displayed as reads per kilobase million (RPKM), thus quantifying gene expression from mRNA sequencing data by normalizing for total read length and the number of sequencing reads.

Reads were mapped to the GRCm38 v96 Ensembl Mus musculus genome using STAR v.2.5.2a (Dobin *et al.*, 2013). The R-package DESeq. 2 v.1.18.1 was used for differential expression analysis (Love et al., 2014). P-values were adjusted using the Benjamini-Hochberg method and genes with adjusted $p<0.05$ were considered statistically significantly regulated. The Reactome pathway (Fabregat *et al.*, 2018) database was used as gene annotation for gene set analysis using the R package PIANO v.1.18.1, with the Stouffer method and Benjamini-Hochberg adjusted p-values.

Single nuclei isolation

Nuclei were isolated from kidney cortex samples from db/m (n = 1) and UNx-Renin mice (n = 2) using Nuclei EZ Lysis Buffer (NUC-101, Sigma-Aldrich) supplemented with Protector RNase Inhibitor (Sigma-Aldrich, 3335399001) (Lysis buffer). Kidney samples were homogenized using a Dounce homogenizer in 1 ml of ice-cold Lysis buffer. The homogenate was incubated on ice for 5 min with an additional 1 ml of Lysis buffer and centrifuged at 500×g for 5 minutes at 4°C. The pellet was resuspended in 500 ul Lysis buffer, and then incubated on ice for 5 minutes and centrifuged at 500×g for 5 minutes at 4°C. The pellet was resuspended in 1000 ul Nuclei Suspension Buffer (NSB - 1x PBS, 1% (w/v) BSA, 0.27% Protector RNase Inhibitor) and centrifuged at 500×g for 5 minutes at 4°C. The pellet was resuspended in 250 ul NSB and filtered through a 40 µM cell strainer (PluriSelect, SKU 43-

10040-50) and an additional 150 ul of NSB was added to the filter. The nuclei enriched in NSB was counted and stained with DRAQ5 (5 µM) (ThermoFishcer Scientific, 62254) for nuclei isolation using the BD FACSAria™ III sorter (70 µm nozzle, 70 psi). 10,000 nuclei were sorted and loaded onto the 10x Chromium (10x Genomics). Library construction was performed using the Chromium Next GEM Single Cell 3' GEM, Library & Gel Bead Kit v3.1 (10x Genomics) according to manufacturer's instructions. The number of cycles used for cDNA amplification was 13. cDNA libraries were sequenced on a NextSeq500 using NextSeq 500/550 High Output Kit v2.5 (150 cycles) (Illumina).

Single-nuclei RNAseq transcriptomic analysis

Reads were mapped to the GRCm38 v96 Ensembl Mus musculus genome using the CellRanger (v. 1.1.0, 10x Genomics) software. Cell Ranger uses Spliced Transcripts Alignment to a Reference (STAR) software to align. For each sample, a count matrix was generated using both intronic and extronic reads. Data processing, including normalization, variance stabilization and dimensionality reduction was performed using the Seurat R package (v. 3.1.1, Stuart *et al.*, 2019). The quality of the data was evaluated using standard RNAseq quality control parameters. Additionally, nuclei with a mitochondrial RNA content of >0.25% were removed from the dataset if more than as nuclei data should not contain any mitochondrial transcripts. The sctransform method was used for data normalization and variance stabilization (Hafemeister and Satija, 2019). To account for sample variance, samples were integrated using 'IntegrateData' function in Seurat. PCA was computed on the integrated dataset and the top 20 PCs was used as input for UMAP dimensionality reduction, where single nuclei can be projected onto a two-dimensional UMAP space for visualization purposes. The integrated dataset was used to select a biological relevant number of clusters, which included determining differential expression between neighbouring clusters, creating a K-nearest neighbour graph and perform modularity optimization (Louvain algorithm).

Differential expression between clusters was calculated using a likelihood-ratio test for single-cell gene expression implemented in Seurat at a family-wise error rate of 5%. Cell identity of the nuclei was determined by examining the most enriched genes in each cluster (marker genes) and compare these with canonical marker genes. To associate bulk gene regulations with a specific cell type, we defined cell type specific genes if the following criteria were fulfilled. (*i*) The gene should have the highest expression level in that cell type, and (*ii*) the gene should have at least 2-fold increased expression compared to the cell type with the second highest expression level.

Statistical Analysis

Results are presented as mean ± standard error of mean (SEM) unless otherwise specified. Except for RNA sequencing data sets, all data was analysed with Graphpad Prism software (version 9.0.0) using either one-way ANOVA with Tukey's post hoc test (body weight, kidney weight and glomerulosclerosis) or two-way ANOVA with Bonferroni's post hoc test (blood glucose and urine ACR). Urine ACR values were log10-transformed before group comparisons. A p-value < 0.05 was considered statistically significant.

ACKNOWLEDGEMENT

The authors would like to acknowledge Henrik Björk Hansen for his help revising the manuscript, and Ida Rune for her help organizing the *in vivo* part of the project, and Malene A. Christensen for skilled technical assistance.

AUTHORS CONTRIBUTIONS STATEMENT

F.S.E., H.M.Æ., A.A.P., M.V.Ø., L.N.F., T.S, J.J., and N.V. designed the study; F.S.E., H.M.Æ., and T.S. performed the experiments; F.S.E., H.M.Æ., T.S., K.G.T.R., and J.C.N. analysed and interpreted the data. F.S.E., J.C.N., and H.M.Æ. drafted the manuscript. F.S.E., J.C.N., H.M.Æ., J.J., T.S., B.F., M.V.Ø., and L.N.F. edited and revised the manuscript; N.V., and J.J. approved the final version of the manuscript.

COMPETING INTERESTS

F.S.E., H.M.Æ., J.C.N., T.S., M.V.Ø., K.T.G.R., and L.N.F. are employees of Gubra ApS; N.V. and J.J. are owners of Gubra ApS.

FUNDING

Frederikke E. Sembach and Helene M. Ægidius were supported by grants from Innovation Fund Denmark.

REFERENCES

Ægidius, H. M. *et al.* (2020) 'Multi-omics characterization of a diet-induced obese model of non-alcoholic steatohepatitis', *Scientific Reports*, 10(1), pp. 1–12. doi: 10.1038/s41598-020-58059-7.

Barwinska, D. *et al.* (2021) 'Molecular characterization of the human kidney interstitium in health and disease', *Science Advances*, 7(7), p. eabd3359. doi: 10.1126/sciadv.abd3359.

Bower, G. *et al.* (1980) 'Studies of the glomerular mesangium and the juxtaglomerular apparatus in the genetically diabetic mouse', *Lab Invest.*, 43(4), pp. 333–41.

Brenner, B. M. *et al.* (2001) 'Effects of Losartan on Renal and Cardiovascular Outcomes in Patients with Type 2 Diabetes and Nephropathy', *New England Journal of Medicine*. doi: 10.1056/nejmoa011161.

Cha, J. J. *et al.* (2013) 'Renal protective effects of toll-like receptor 4 signaling blockade in type 2 diabetic mice', *Endocrinology*, 154(6), pp. 2144–2155. doi: 10.1210/en.2012-2080.

Conesa, A. *et al.* (2016) 'A survey of best practices for RNA-seq data analysis', *Genome Biology*. doi: 10.1186/s13059-016-0881-8.

Dobin, A. *et al.* (2013) 'STAR: Ultrafast universal RNA-seq aligner', *Bioinformatics.*, 29(1), pp. 15–21. doi: 10.1093/bioinformatics/bts635.

Dong, M. *et al.* (2021) 'SCDC: bulk gene expression deconvolution by multiple single-cell RNA sequencing references', *Briefings in bioinformatics*, 22(1), pp. 416–427. doi: 10.1093/bib/bbz166.

Fabregat, A. *et al.* (2018) 'The Reactome Pathway Knowledgebase', *Nucleic Acids Research*. Oxford University Press, 46, pp. D649–D655. doi: 10.1093/nar/gkx1132.

Fan, Y. *et al.* (2019) 'Comparison of kidney transcriptomic profiles of early and advanced diabetic nephropathy reveals potential new mechanisms for disease progression', *Diabetes*. doi: 10.2337/db19-0204.

Fioretto, P. and Mauer, M. (2007) 'Histopathology of diabetic nephropathy', *Semin Nephrol.*, 27(2), pp. 195–207. doi: 10.1016/j.semnephrol.2007.01.012.HISTOPATHOLOGY.

Fu, J. *et al.* (2019) 'Single-cell RNA profiling of glomerular cells shows dynamic changes in experimental diabetic kidney disease', *Journal of the American Society of Nephrology*. doi: 10.1681/ASN.2018090896.

Granqvist, A. B. *et al.* (2020) 'High protein diet accelerates diabetes and kidney disease in the BTBR ob/ob mouse', *American Journal of Physiology - Renal Physiology*, 318(3), pp. F763–F771. doi: 10.1152/AJPRENAL.00484.2019.

Hafemeister, C. and Satija, R. (2019) 'Normalization and variance stabilization of single-cell RNA-seq data using regularized negative binomial regression', *bioRxiv*. Genome Biology, p. 576827. doi: 10.1101/576827.

Harlan, S. M., Heinz-Taheny, K. M., Overstreet, J. M., *et al.* (2018) 'Pathological and Transcriptome Changes in the ReninAAV db/db uNx Model of Advanced Diabetic Kidney Disease Exhibit Features of Human Disease', *Toxicologic Pathology*, 46(8), pp. 991–998. doi: 10.1177/0192623318804986.

Harlan, S. M., Heinz-Taheny, K. M., Sullivan, J. M., *et al.* (2018) 'Progressive Renal Disease Established by Renin-Coding Adeno-Associated Virus–Driven Hypertension in Diverse Diabetic Models', *Journal of the American Society of Nephrology*, 29(2), pp. 477–491. doi: 10.1681/asn.2017040385.

Heerspink, H. J. L. *et al.* (2019) 'Canagliflozin reduces inflammation and fibrosis biomarkers: a potential mechanism of action for beneficial effects of SGLT2 inhibitors in diabetic kidney disease', *Diabetologia*. doi: 10.1007/s00125-019-4859-4.

Heerspink, H. J. L. *et al.* (2020) 'Dapagliflozin in Patients with Chronic Kidney Disease', *New England Journal of Medicine*. doi: 10.1056/nejmoa2024816.

Jensen, T. *et al.* (1989) 'FEATURES OF ENDOTHELIAL DYSFUNCTION IN EARLY DIABETIC NEPHROPATHY', *The Lancet*. doi: 10.1016/S0140-6736(89)91365-2.

Jourde-Chiche, N. *et al.* (2019) 'Endothelium structure and function in kidney health and disease', *Nature Reviews Nephrology*. doi: 10.1038/s41581-018-0098-z.

Ju, W. *et al.* (2013) 'Defining cell-type specificity at the transcriptional level in human disease', *Genome Research*, 23(11), pp. 1862–1873. doi: 10.1101/gr.155697.113.

Kramer, A. *et al.* (2019) 'The European Renal Association – European Dialysis and Transplant Association (ERA-EDTA) Registry Annual Report 2016: a summary', *Clinical Kidney Journal*, pp. 1–19.

Levin, A. *et al.* (2020) 'Novel insights into the disease transcriptome of human diabetic glomeruli and tubulointerstitium', *Nephrology, dialysis, transplantation*, 35(12), pp. 2059–2072. doi: 10.1093/ndt/gfaa121.

Levine, D. Z., Iacovitti, M. and Robertson, S. J. (2008) 'Modulation of single-nephron GFR in the db/db mouse model of type 2 diabetes mellitus. II. Effects of renal mass reduction', *American Journal of Physiology - Regulatory Integrative and Comparative Physiology*, 294(6), pp. 1840–1846. doi: 10.1152/ajpregu.00457.2007.

Lewis, E. J. *et al.* (1993) 'The Effect of Angiotensin-Converting-Enzyme Inhibition on Diabetic Nephropathy', *New England Journal of Medicine*, 329, pp. 1456–62.

Lin, M. *et al.* (2013) 'The TLR4 antagonist CRX-526 protects against advanced diabetic nephropathy', *Kidney International*. Elsevier Masson SAS, 83(5), pp. 887–900. doi: 10.1038/ki.2013.11.

Long, A. N. and Dagogo-JAck, S. (2011) 'The Cormobidities of Diabetes and Hypertension: Mechanisms and Approach to Target Organ Protection', *J Clin Hypertens*, 13(4), pp. 244–251. doi: 10.1111/j.1751-7176.2011.00434.x.The.

Mann, J. F. E. *et al.* (2017) 'Liraglutide and renal outcomes in type 2 diabetes', *New England Journal of Medicine*, 377(9), pp. 839–848. doi: 10.1056/NEJMoa1616011.

McCullough, K. P. *et al.* (2019) 'Projecting ESRD incidence and prevalence in the United States through 2030', *Journal of the American Society of Nephrology*. doi: 10.1681/ASN.2018050531.

Nguyen, D. *et al.* (2006) 'Macrophage accumulation in human progressive diabetic nephropathy', *Nephrology*, 11(3), pp. 226–231. doi: 10.1111/j.1440-1797.2006.00576.x.

Ninichuk, V., Kulkarni, O., Clauss, S. and Anders, H. J. (2007) 'Tubular atrophy, interstitial fibrosis, and inflammation in type 2 diabetic db/db mice. An accelerated model of advanced diabetic nephropathy.', *Eur J Med Res.*, 12, pp. 351–355.

Ninichuk, V., Kulkarni, O., Clauss, S. and Anders, H.-J. (2007) 'Tubular atrophy, interstitial fibrosis, and inflammation in type 2 diabetic db/db mice. An accelerated model of advanced diabetic nephropathy.', *European journal of medical research*, 12(8), pp. 351–5. Available at: http://www.ncbi.nlm.nih.gov/pubmed/17933712.

Omote, K. *et al.* (2014) 'Role of the TNF pathway in the progression of diabetic nephropathy in KK-Ay mice', *American Journal of Physiology - Renal Physiology*, 306(11), pp. 1335–1347. doi: 10.1152/ajprenal.00509.2013.

Østergaard, M. V. *et al.* (2021) 'Therapeutic effects of lisinopril and empagliflozin in a mouse model of hypertension-accelerated diabetic kidney disease', *American Journal of Physiology - Renal Physiology (in press)*. doi: https://doi.org/10.1152/ajprenal.00154.2021.

Paulsen, S. J. *et al.* (2009) 'Gene expression profiling of individual hypothalamic nuclei from single animals using laser capture microdissection and microarrays', *Journal of Neuroscience Methods*, 177(1), pp. 87–93. doi: 10.1016/j.jneumeth.2008.09.024.

Perkovic, V. *et al.* (2019) 'Canagliflozin and Renal Outcomes in Type 2 Diabetes and Nephropathy', *New England Journal of Medicine.*, 380, pp. 2295–2306. doi: 10.1056/NEJMoa1811744.

Pichler, R. *et al.* (2017) 'Immunity and inflammation in diabetic kidney disease: Translating mechanisms to biomarkers and treatment targets', *American Journal of Physiology - Renal Physiology*, 312(4), pp. F716–F731. doi: 10.1152/ajprenal.00314.2016.

Schmid, H. *et al.* (2006) 'Modular activation of nuclear factor-κB transcriptional programs in human diabetic nephropathy', *Diabetes*, 55(11), pp. 2993–3003. doi: 10.2337/db06-0477.

Sembach, F. E. *et al.* (2019) 'Impact of sex on diabetic nephropathy and the renal transcriptome in UNx db/db C57BLKS mice', *Physiological Reports*, 7(24). doi: 10.14814/phy2.14333.

Sircar, M. *et al.* (2018) 'Complement 7 Is Up-Regulated in Human Early Diabetic Kidney Disease', *American Journal of Pathology*. American Society for Investigative Pathology, 188(10), pp. 2147–2154. doi: 10.1016/j.ajpath.2018.06.018.

Sokolowski, D. J. *et al.* (2021) 'Single-cell mapper (scMappR): using scRNA-seq to infer the cell-type specificities of differentially expressed genes'. Oxford University Press, 3(1), pp. 1–19. doi: 10.1093/nargab/lqab011.

Stuart, T. *et al.* (2019) 'Comprehensive Integration of Single-Cell Data', *Cell*. Elsevier Inc., 177, pp. 1888–1902. doi: 10.1016/j.cell.2019.05.031.

Susztak, K. *et al.* (2006) 'Glucose-Induced Reactive Oxygen Species Cause Apoptosis of Podocytes and Podocyte Depletion at the Onset of Diabetic Nephropathy', 55(January), pp. 225–233.

Tang, S. C. W. and Yiu, W. H. (2020) 'Innate immunity in diabetic kidney disease', *Nature Reviews Nephrology*. Springer US, 16(4), pp. 206–222. doi: 10.1038/s41581-019-0234-4.

Tang, S. M. *et al.* (2020) 'Identification of C3 as a therapeutic target for diabetic nephropathy by bioinformatics analysis', *Scientific Reports*. Nature Publishing Group UK, 10(1), pp. 1–12. doi: 10.1038/s41598-020-70540-x.

Tervaert, T. W. C. *et al.* (2010) 'Pathologic classification of diabetic nephropathy', *Journal of the American Society of Nephrology*, 21, pp. 556–563. doi: 10.1681/ASN.2010010010.

United States Renal Data System (2018) *2018 USRDS ANNUAL DATA REPORT | VOLUME 2 – End Stage Renal Disease in the United States*, *National Institutes of Health, National Institute of Diabetes and Digestive and Kidney Diseases*.

Verzola, D. *et al.* (2014) 'Enhanced glomerular Toll-like receptor 4 expression and signaling in patients with type 2 diabetic nephropathy and microalbuminuria', *Kidney International*. Elsevier Masson SAS, 86(6), pp. 1229–1243. doi: 10.1038/ki.2014.116.

Wang, T. *et al.* (2019) 'Comparative analysis of differential gene expression analysis tools for single-cell RNA sequencing data', *BMC Bioinformtics*, pp. 1–16.

Wanner, C. *et al.* (2016) 'Empagliflozin and progression of kidney disease in type 2 diabetes', *New England Journal of Medicine*. doi: 10.1056/NEJMoa1515920.

Wilson, P. C. *et al.* (2019) 'The single-cell transcriptomic landscape of early human diabetic nephropathy', *Proceedings of the National Academy of Sciences of the United States of America*, 116(39), pp. 19619–19625. doi: 10.1073/pnas.1908706116.

Wong, C. K. *et al.* (2008) 'Aberrant expression of soluble co-stimulatory molecules and adhesion molecules in type 2 diabetic patients with nephropathy', *Journal of Clinical Immunology*, 28(1), pp. 36–43. doi: 10.1007/s10875-007-9137-4.

Woroniecka, K. I. *et al.* (2011) 'Transcriptome analysis of human diabetic kidney disease', *Diabetes*. doi: 10.2337/db10-1181.

Yiu, W. H. *et al.* (2018) 'Complement C5a inhibition moderates lipid metabolism and reduces tubulointerstitial fibrosis in diabetic nephropathy', *Nephrology Dialysis Transplantation*, 33(8), pp. 1323–1332. doi: 10.1093/ndt/gfx336.

Zhang, C. *et al.* (2019) 'The preprohormone expression profile of enteroendocrine cells following Roux-en-Y gastric bypass in rats', *Peptides*. Elsevier, 118. doi: 10.1016/j.peptides.2019.170100.

FIGURES

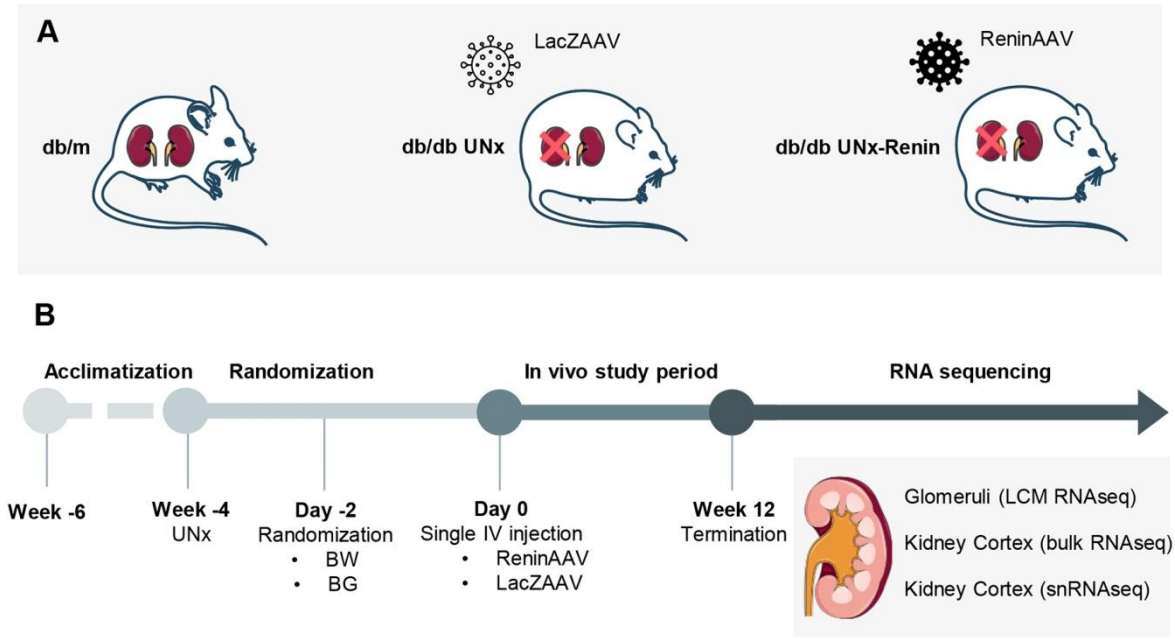

Figure 1. Graphic illustration of the study outline. (A) Study groups. (B) Study outline. The top and bottom parts of the kidney cortex were sequestered for bulk and single-nucleus RNA sequencing. The remaining part of the kidney cortex was cryosectioned and glomeruli were isolated using laser-capture microdissection. AAV, adeno-associated virus; BG, blood glucose; BW, body weight; LCM, laser-capture microdissection; snRNAseq, single-nucleus RNA sequencing; UNx, uninephrectomy.

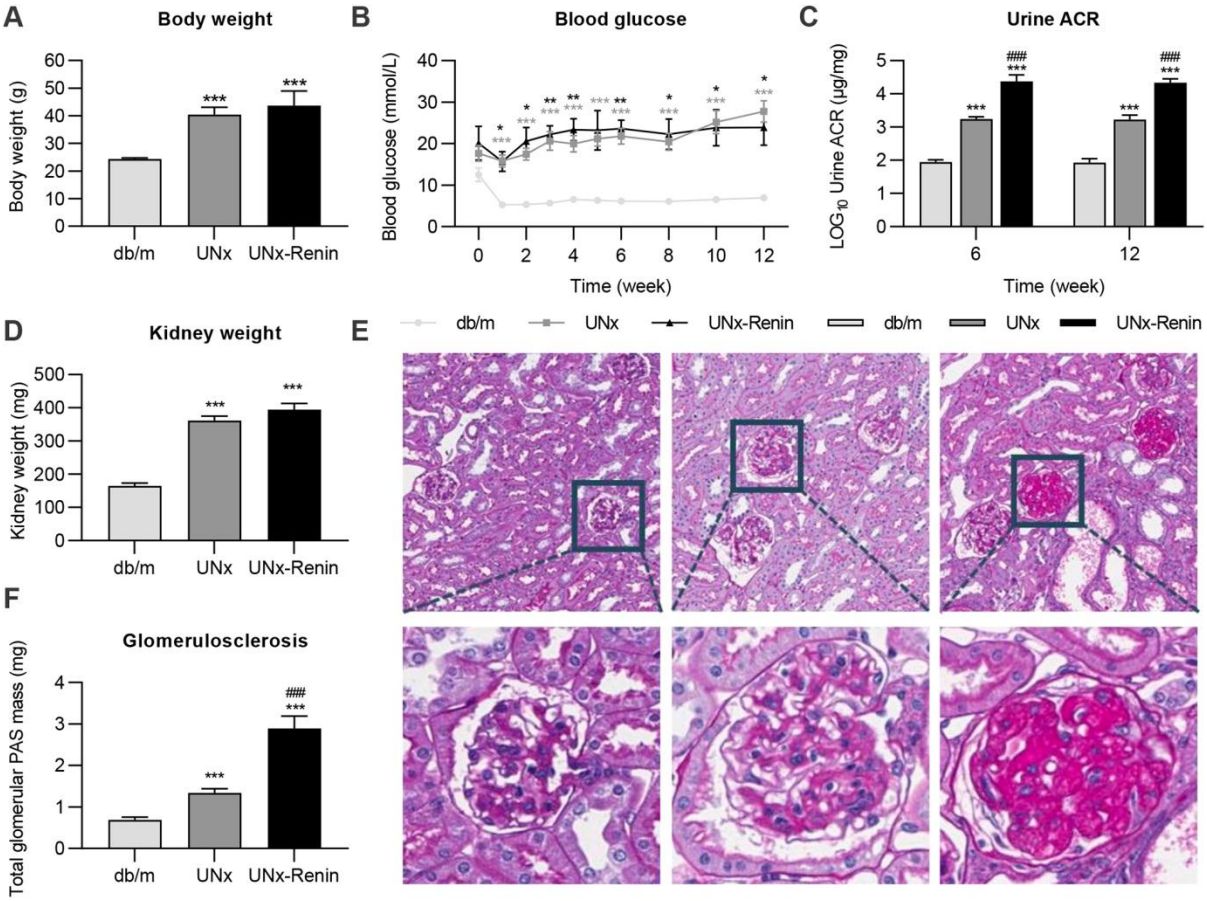

Figure 2. Measurements 12 weeks after injection with ReninAAV or LacZAAV in diabetic UNx mice and age-matched db/m controls. (A) Body weight. (B) Blood glucose measured biweekly throughout the study. (C) LOG10-transformed urine albumin-to-creatinine ratio (ACR) at week 6 and 12 in the study. (D) Kidney weight. (E) Representative images of PAS-stained kidney sections with magnified images of glomeruli. (F) Quantification of glomerulosclerosis. Data is presented as mean ± SEM (n = 5-13). One-way ANOVA with Tukey's post hoc test (Fig. 1A, D and F) or two-way ANOVA with Bonferroni's post hoc test (Fig. 1B and C). *:P < 0.05, **:P < 0.01, ***: P < 0.001 compared to db/m. ###: P < 0.001 compared to UNx.

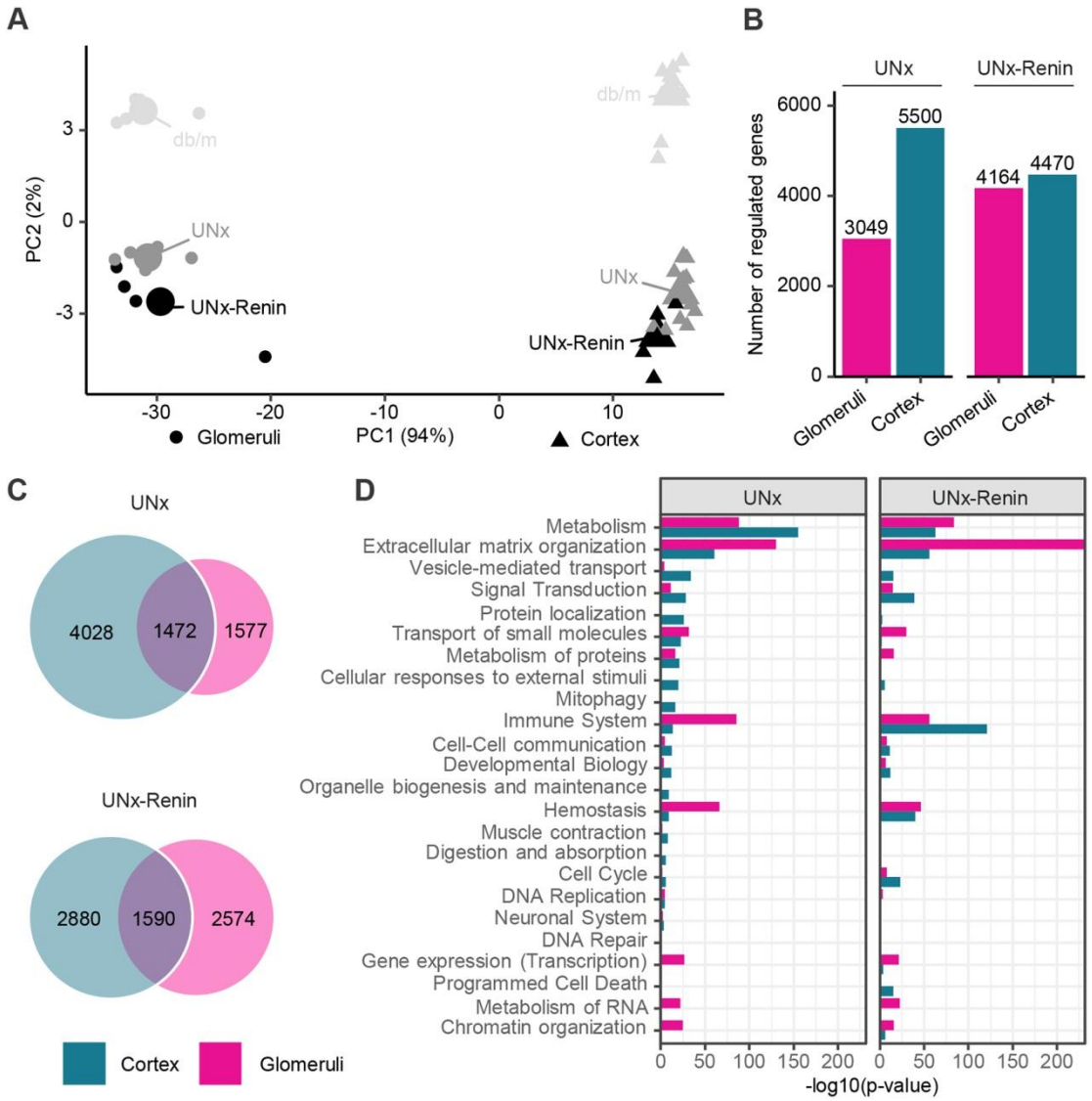

Figure 3. Highly specific gene expression profiles in glomeruli versus cortex for UNx and UNx-Renin mice compared to db/m controls. (A) Principal component (PC) analysis of the 500 most variable genes. Small points indicate a sample and large points the group centre. (B) Total number of differentially expressed genes (DEGs) in glomeruli and kidney cortex from UNx and UNx-Renin mice compared with db/m controls, respectively. (C) Venn diagrams depicting shared and separate DEGs in glomeruli and kidney cortex from UNx or UNx-Renin mice, respectively. (D) Reactome pathway gene enrichment analysis in glomeruli and kidney cortex from UNx or UNx-Renin mice. Degree of perturbation is presented as the −log10(p-value) after correction for gene-wise multiple testing (n=5-13).

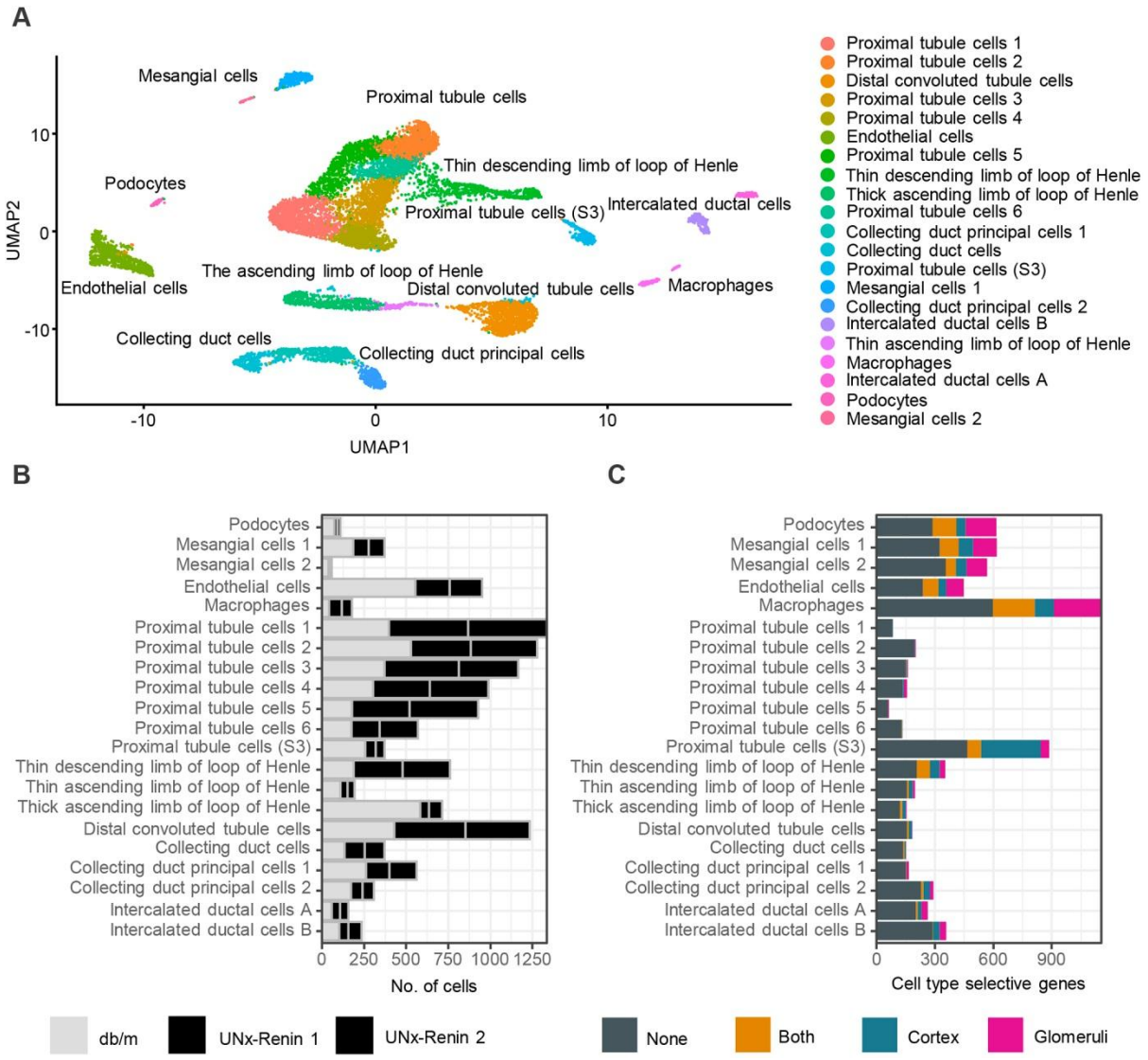

Figure 4. Number of DEGs in cortex and glomeruli of UNx-Renin mice mapped to a specific cell type using single-nucleus RNAseq. (A) UMAP (Uniform Manifold Approximation and Projection) of 12.840 nuclei from mainly kidney cortex of db/m and UNx-Renin mice (n = 1-2). Each dot represents a nucleus coming from a single cell. Cells that show similar transcriptomic profiles are grouped by colour based on unsupervised clustering. 21 cell populations were identified. (B) Number of cells found in each cell population per animal. (C) Number of cell type specific genes significantly regulated between UNx-Renin and db/m mice in glomeruli, cortex, both or none of the two tissue areas, respectively. Genes were defined as specific to a cell population, if the expression was increased by 2-fold as compared to the cell population with the second highest expression level.

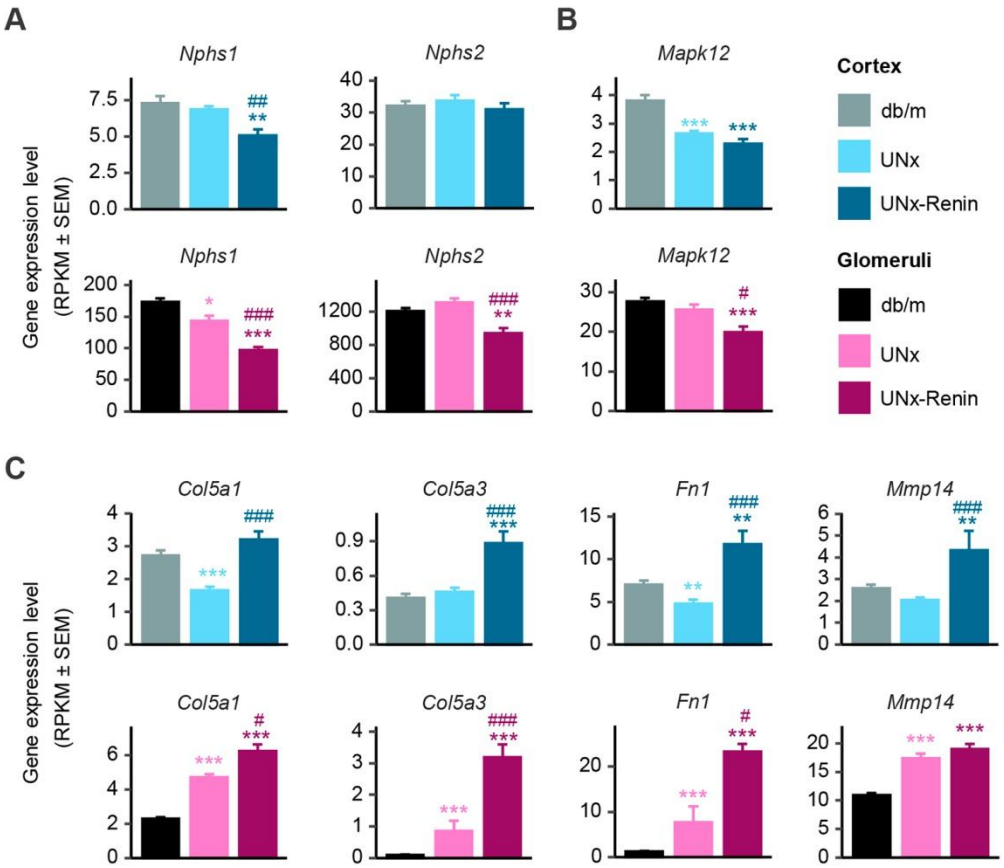

Figure 5. Regulation of cell type specific genes in cortex and glomeruli of UNx-Renin mice. Expression levels presented as mean ± SEM RPKM values for genes in (A) Nephrin Family Interactions (*Nphs1, Nphs1*), (B) Myogenesis (*Mapk12*) and (C) Degradation of ECM (*Col5a1, Col5a3, Fn1, Mmp14*) pathways. *:P < 0.05, **:P < 0.01, ***: P < 0.001 compared to db/m. #:P < 0.05, ##:P < 0.01, ###: P < 0.001 compared to UNx (False discovery rate adjusted p-values, n=5-13).

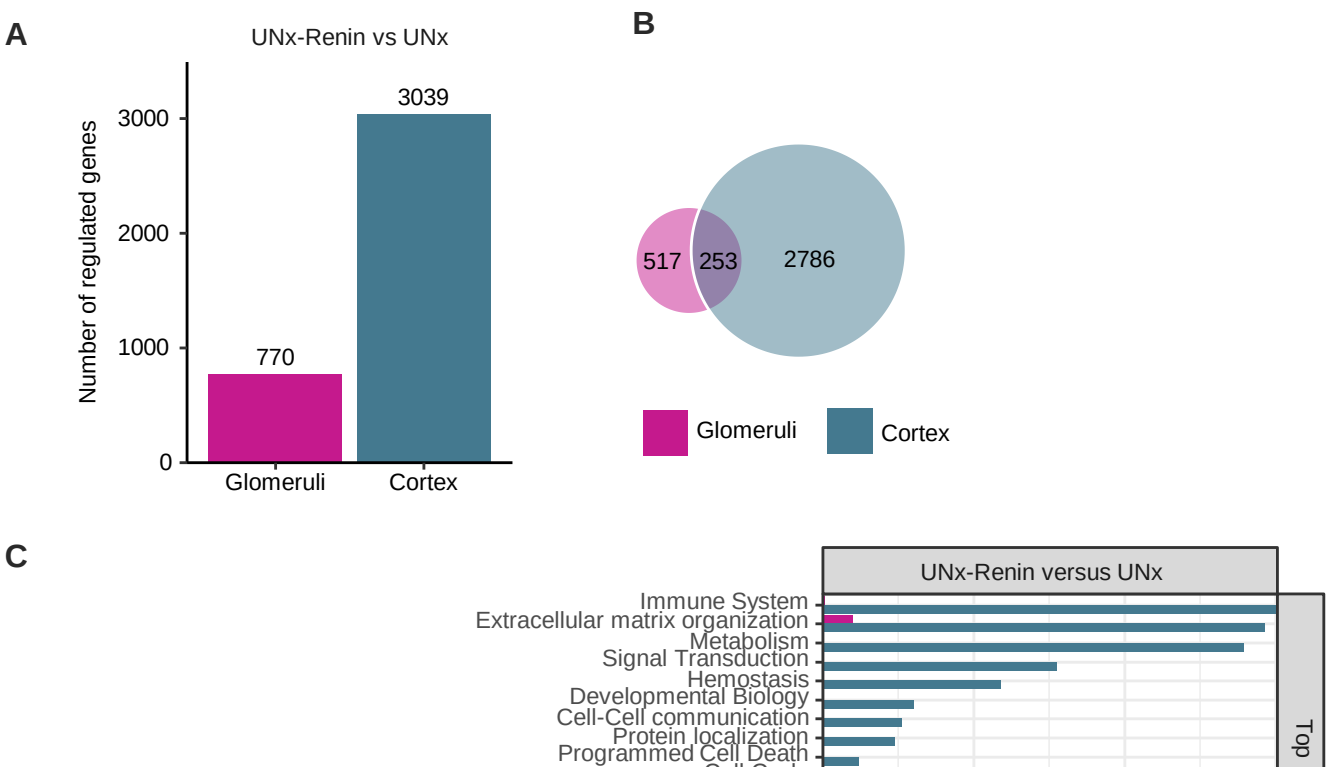

Fig. S1. Differentially expressed genes and gene enrichment analysis using Reactome for UNx-Renin mice compared to UNx mice in both glomeruli and kidney cortex samples. Degree of perturbation is presented as the −log10(p-value) after correction for gene-wise multiple testing (n=5-13).

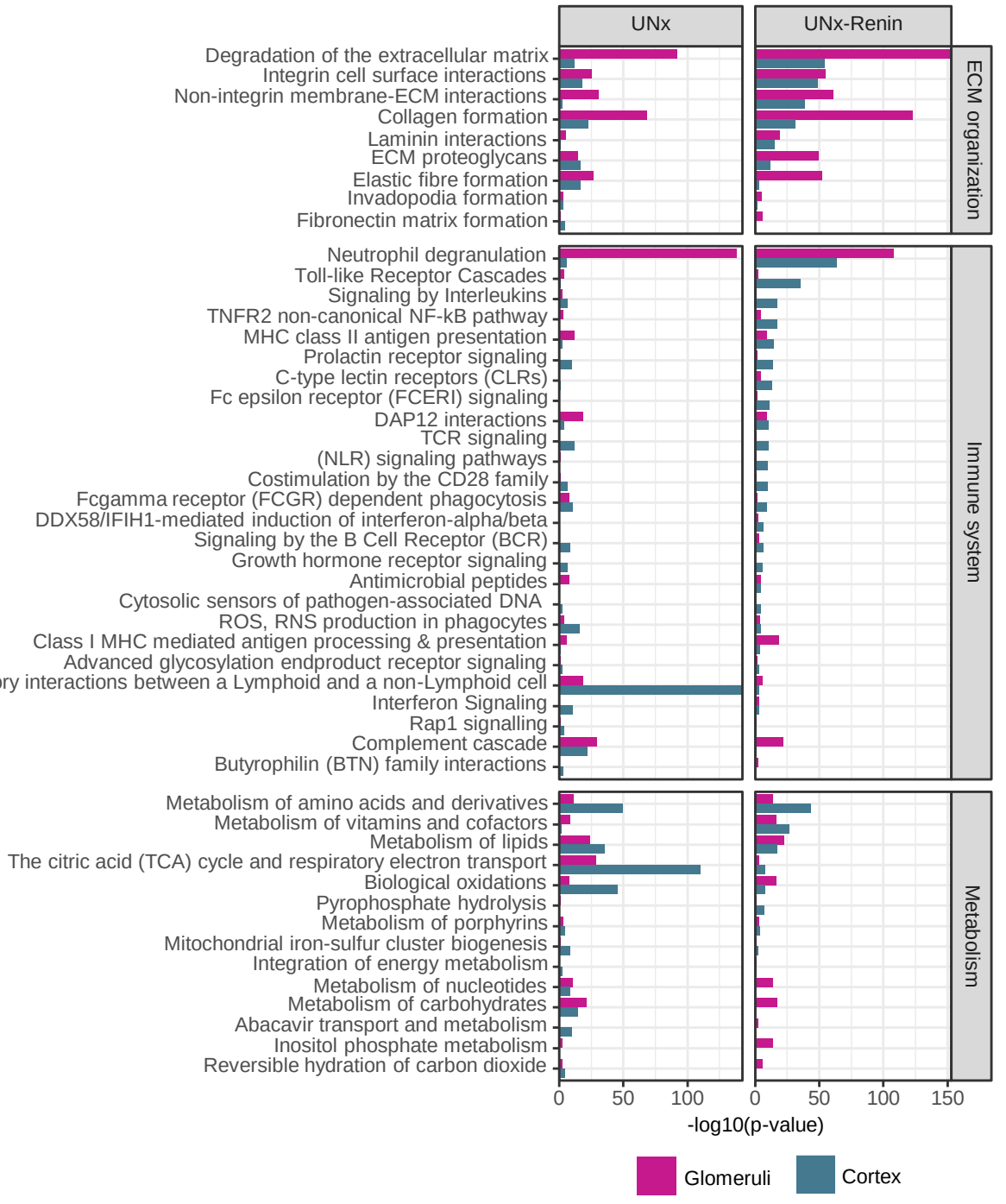

Fig. S2. Gene enrichment analysis using Reactome of sub-pathways for UNx or UNx-Renin mice compared to db/m controls. Degree of perturbation is presented as the −log10(p-value) after correction for gene-wise multiple testing (n=5-13).

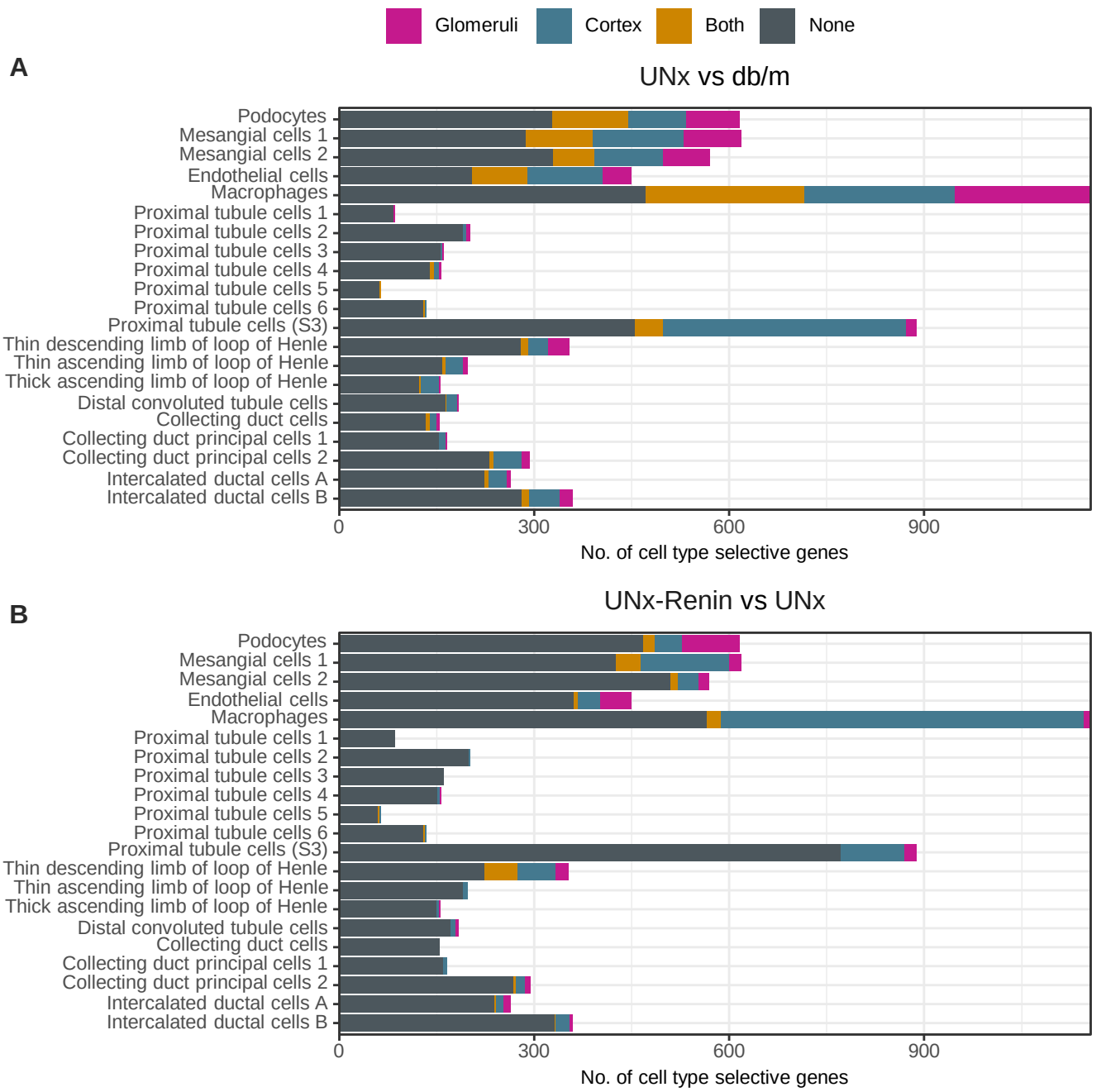

Fig. S3. Number of cell type specific DEGs between UNx mice and db/m controls, or between UNx-Renin and UNx mice, in glomeruli, cortex, both or none of the two tissue areas. Genes were defined as specific to the cell population with the highest average expression level, if the expression level was increased by 2-fold as compared to the cell population with the second highest expression level.

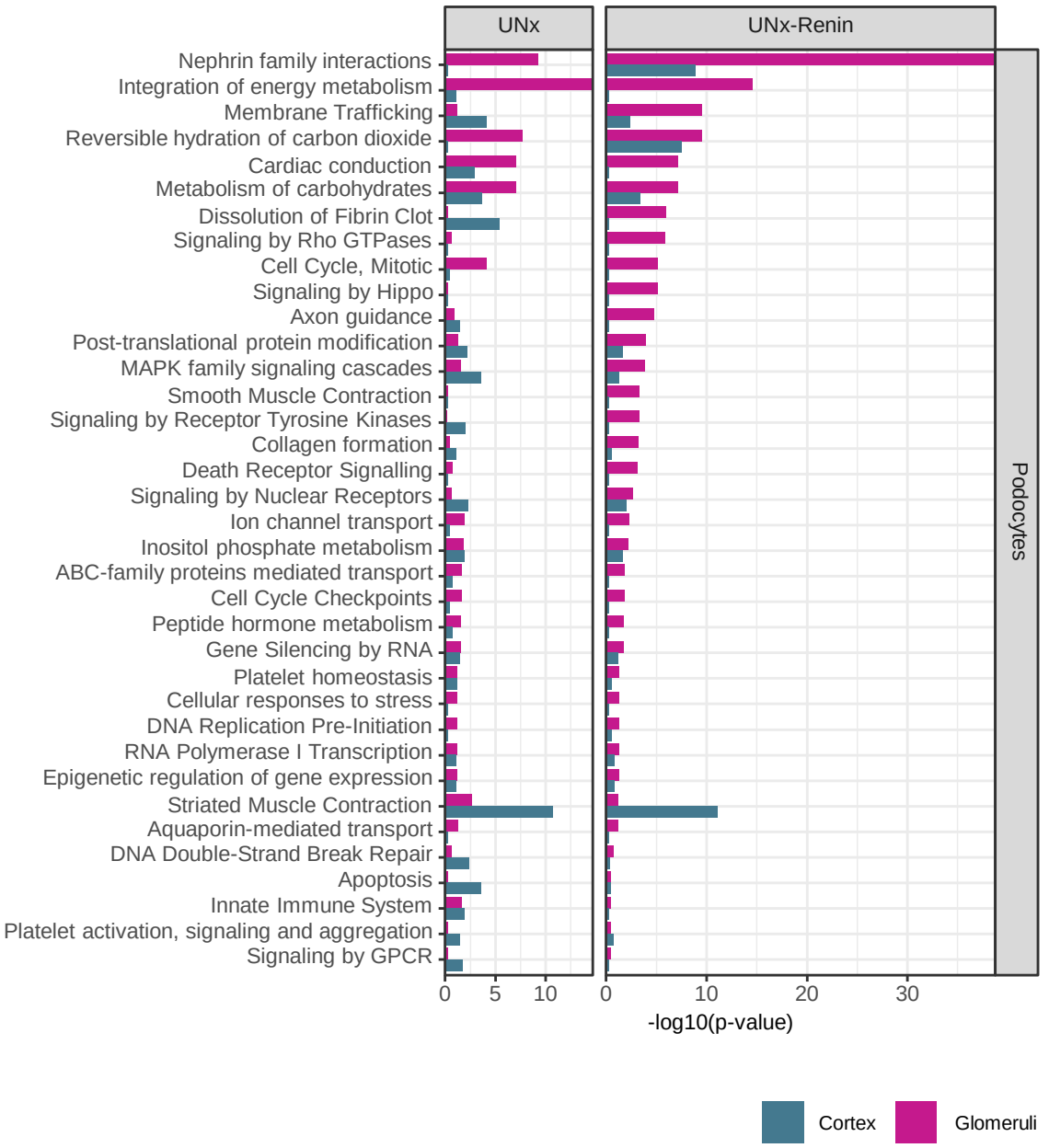

Fig. S4. Podocyte- specific DEGs found in kidney cortex and glomeruli of UNx and UNx-Renin mice compared to db/m controls. Degree of perturbation is presented as the −log10(p-value) after correction for gene-wise multiple testing (n=5-13).

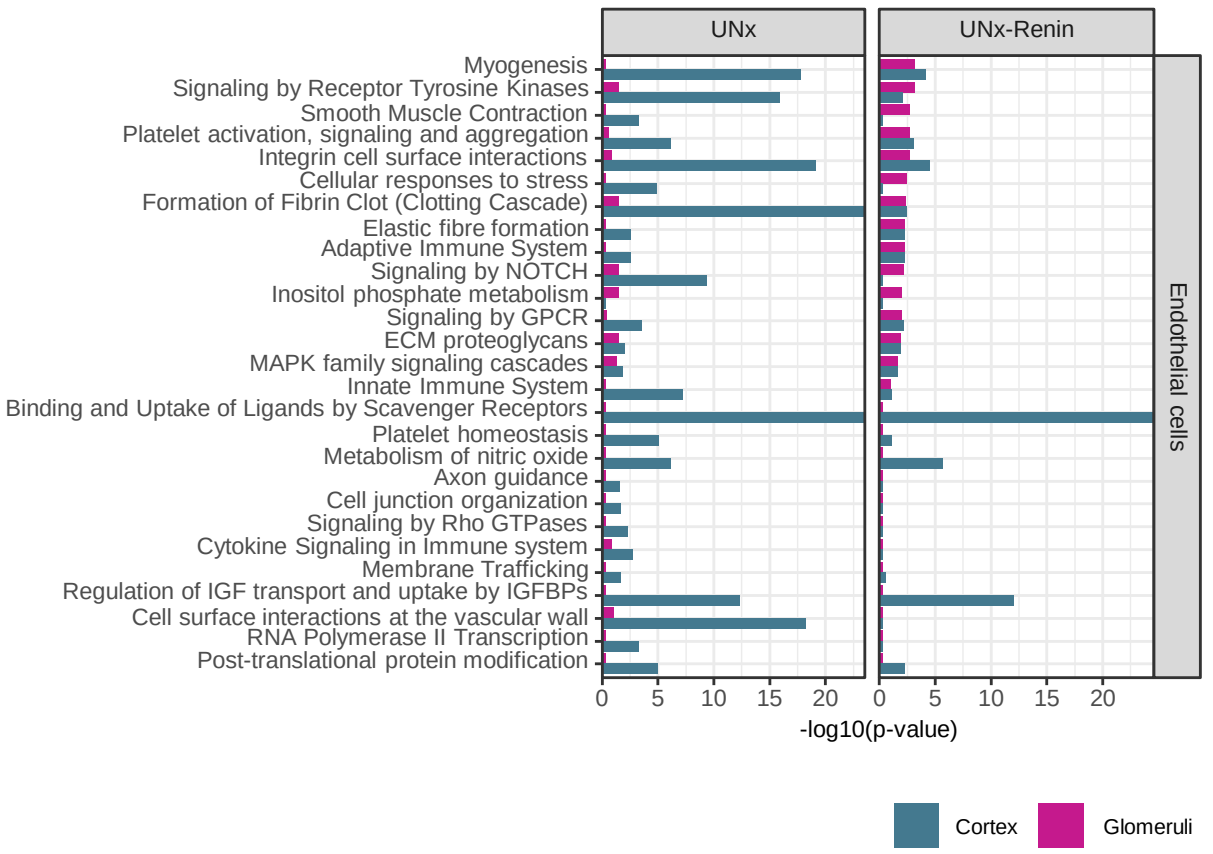

Fig. S5. Endothelial cell- specific DEGs found in kidney cortex and glomeruli of UNx and UNx-Renin mice compared to db/m controls. Degree of perturbation is presented as the −log10(p-value) after correction for gene-wise multiple testing (n=5-13).

Fig. S6. Mesangial cell- specific DEGs found in kidney cortex and glomeruli of UNx and UNx-Renin mice compared to db/m controls. Degree of perturbation is presented as the −log10(p-value) after correction for gene-wise multiple testing (n=5-13).

Table S1. Selected differential expressed genes (DEGs) in kidney cortex

Summary of selected DEGs in kidney cortex and comparison to relevant transcriptomic studies of human DKD (Woroniecka *et al.*, 2011; Ju *et al.*, 2013; Levin *et al.*, 2020; Fan *et al.*, 2019; Verzola *et al*., 2014; Sircar *et al.*, 2018) including use of the Nephroseq database. Fold change, FC; NA, not applicable; NS, non-significant.

Gene Name	Gene Description	UNx vs db/m	UNx-Renin vs db/m	UNx-Renin vs UNx	Human DKD Transcriptomics
		Log_2 FC (p-value)	Log_2 FC (p-value)	Log_2 FC (p-value)	
Adamts4	a disintegrin-like and metallopeptidase (reprolysin type) with thrombospondin type 1 motif, 4	0.5 (0.13)	1.3 (0.001)	0.8 (0.07)	NA
C3	complement component 3	0.0 (0.87)	1.8 (5.54E-11)	1.8 (7.08E-11)	Upregulated in tubulointerstitium in Woroniecka *et al.*, 2011 and Ju *et al.*, 2013.
C6	complement component 6	1.3 (0.0006)	2.7 (3.09E-10)	1.4 (0.002)	Upregulated in tubulointerstitium in Woroniecka *et al.*, 2011 and Ju *et al.*, 2013.
C7	complement component 7	0.9 (0.0004)	1.9 (1.98E-08)	1.0 (0.01)	Upregulated in tubulointerstitium in Woroniecka *et al.*, 2011; Ju *et al.*, 2013 and Sircar *et al.*, 2018.
Col1a1	collagen, type I, alpha 1	-0.9 (0.01)	1.1 (0.03)	2.0 (2.49E-05)	Upregulated in tubulointerstitium in Woroniecka *et al.*, 2011; Ju *et al.*, 2013 and Levin *et al.*, 2020.
Col3a1	collagen, type III, alpha 1	-1.4 (2.26E-05)	0.6 (0.25)	2.0 (1.38E-05)	Upregulated in tubulointerstitium in Woroniecka *et al.*, 2011 and Ju *et al.*, 2013.
Col5a1	collagen, type V, alpha 1	-0.7 (2.47E-08)	0.2 (0.25)	0.9 (6.83E-08)	Upregulated in tubulointerstitium in Woroniecka *et al.*, 2011 and Ju *et al.*, 2013.
Col5a3	collagen, type V, alpha 3	0.2 (0.47)	1.1 (7.61E-06)	0.9 (0.0004)	NS regulated in Ju *et al.*, 2013, while downregulated in Woroniecka *et al.*, 2011.

Col6a1	collagen, type VI, alpha 1	-0.2 (0.09)	0.6 (0.0001)	0.9 (2.36E-07)	Downregulated in tubulointerstitium in Woroniecka *et al.*, 2011 and Ju *et al.*, 2013.
Col6a2	collagen, type VI, alpha 2	-0.2 (0.24)	0.9 (6.16E-06)	1.1 (4.98E-08)	Upregulated in tubulointerstitium in Woroniecka *et al.*, 2011 and NS regulated in Ju *et al.*, 2013.
Cxcl1	chemokine (C-X-C motif) ligand 1	1.2 (0.08)	3.8 (3.23E-06)	2.6 (0.003)	Upregulated in whole kidney in Fan *et al.*, 2019 and in tubulointerstitium in Woroniecka *et al.*, 2011 and Ju *et al.*, 2013.
Cxcl2	chemokine (C-X-C motif) ligand 2	1.0 (0.21)	5.1 (2.28E-13)	4.2 (5.50E-10)	Downregulated in whole kidney in Fan *et al.*, 2019 and NS regulated in tubulointerstitium in Woroniecka *et al.*, 2011 and Ju *et al.*, 2013.
Cyp2d9	cytochrome P450, family 2, subfamily d, polypeptide 9	2.8 (3.72E-50)	2.4 (1.60E-20)	-0.4 (0.20)	NA
Fn1	fibronectin 1	-0.5 (0.008)	0.7 (0.008)	1.3 (2.25E-06)	Upregulated in tubulointerstitium in Woroniecka *et al.*, 2011 and Ju *et al.*, 2013.
Lox	lysyl oxidase	0.1 (0.81)	1.4 (8.50E-07)	1.3 (8.62E-06)	NS regulated in tubulointerstitium in Woroniecka *et al.*, 2011, while downregulated in Ju *et al.*, 2013.
Mapk12	mitogen-activated protein kinase 12	-0.5 (7.55E-08)	-0.7 (1.64E-08)	-0.2 (0.18)	NS regulated in tubulointerstitium in Ju *et al.*, 2013.
Mmp12	matrix metallopeptidase 12	0.8 (0.02)	3.2 (3.22E-23)	2.4 (2.78E-14)	NS regulated in tubulointerstitium in Woroniecka *et al.*, 2011 and Ju *et al.*, 2013.
Mmp14	matrix metallopeptidase 14 (membrane-inserted)	-0.3 (0.06)	0.7 (0.001)	1.1 (2.05E-06)	NS regulated in tubulointerstitium in Ju *et al.*, 2013, while downregulated in Woroniecka *et al.*, 2011.
Mmp3	matrix metallopeptidase 3	-0.1 (0.86)	1.1 (0.16)	1.3 (0.13)	NS regulated in tubulointerstitium in Woroniecka *et al.*, 2011 and Ju *et al.*, 2013.

Mmp7	matrix metallopeptidase 7	-2.1 (0.16)	2.7 (0.15)	4.8 (0.01)	Upregulated in whole kidney in Fan *et al.*, 2019 and in tubulointerstitium in Woroniecka *et al.*, 2011 and Ju *et al.*, 2013.
Mmp8	matrix metallopeptidase 8	0.9 (0.42)	2.2 (0.08)	1.2 (0.36)	NS regulated in tubulointerstitium in Ju *et al.*, 2013, while downregulated in Woroniecka *et al.*, 2011.
Nphs1	nephrosis 1, nephrin	-0.1 (0.59)	-0.5 (0.001)	-0.4 (0.01)	Downregulated in tubulointerstitium in Woroniecka *et al.*, 2011 and Ju *et al.*, 2013.
Nphs2	nephrosis 2, podocin	0.1 (0.58)	-0.1 (0.81)	-0.1 (0.50)	NS regulated in tubulointerstitium in Woroniecka *et al.*, 2011, while downregulated in Ju *et al.*, 2013.
Rbp2	retinol binding protein 2, cellular	3.4 (0.0003)	2.7 (0.04)	-0.7 (0.63)	NA
Serpine1	serine (or cysteine) peptidase inhibitor, clade E, member 1	0.0 (0.89)	1.1 (0.0001)	1.0 (0.0004)	Downregulated in tubulointerstitium in Woroniecka *et al.*, 2011 and Ju *et al.*, 2013.
Timp1	tissue inhibitor of metalloproteinase 1	-0.6 (0.51)	2.1 (0.04)	2.6 (0.008)	Upregulated in tubulointerstitium in Woroniecka *et al.*, 2011 and Ju *et al.*, 2013.
Tlr4	toll-like receptor 4	-0.1 (0.52)	0.6 (0.03)	0.7 (0.006)	Upregulated in tubulointerstitium in Verzola *et al*., 2014, and Ju *et al.,* 2013.
Ugt1a10	UDP glycosyltransferase 1 family, polypeptide A10	1.8 (3.58E-30)	1.8 (2.08E-18)	0.1 (0.88)	NA
Vcam1	vascular cell adhesion molecule 1	-0.4 (0.02)	2.4 (3.57E-29)	2.8 (2.53E-40)	Upregulated in tubulointerstitium in Woroniecka *et al.*, 2011 and Ju *et al.*, 2013.

Table S2. Selected differential expressed genes (DEGs) in glomeruli

Summary of selected DEGs in glomeruli and comparison to relevant transcriptomic studies of human DKD (Woroniecka *et al.*, 2011; Ju *et al.*, 2013; Levin *et al.*, 2020; Verzola *et al.*, 2014) including use of the Nephroseq database. Fold change, FC; NA, not applicable; NS, non-significant.

Gene Name	Gene Description	UNx vs db/m	UNx-Renin vs db/m	UNx-Renin vs UNx	Comments
		Log_2 FC (p-value)	Log_2 FC (p-value)	Log_2 FC (p-value)	
Adamts4	a disintegrin-like and metallopeptidase (reprolysin type) with thrombospondin type 1 motif, 4	3.8 (1.39E-11)	3.4 (1.89E-09)	-0.4 (0.74)	NA
C3	complement component 3	-0.1 (0.94)	2.2 (1.48E-05)	2.3 (5.39E-05)	Upregulated in glomeruli in Woroniecka *et al.*, 2011; Ju *et al.*, 2013 and Levin *et al.*, 2020.
C6	complement component 6	5.2 (1.22E-08)	3.0 (0.003)	-2.2 (0.03)	NS regulated in glomeruli in Woroniecka *et al.*, 2011, while downregulated in Ju et al., 2013.
C7	complement component 7	1.4 (0.30)	2.1 (0.08)	0.6 (0.81)	Upregulated in glomeruli in Woroniecka *et al.*, 2011, while NS regulated in Ju et al., 2013.
Col1a1	collagen, type I, alpha 1	1.1 (0.37)	2.7 (0.003)	1.7 (0.25)	Upregulated in glomeruli in Woroniecka *et al.*, 2011; Ju *et al.*, 2013 and Levin *et al.*, 2020.
Col3a1	collagen, type III, alpha 1	0.7 (0.12)	2.1 (8.98E-09)	1.4 (0.002)	Upregulated in glomeruli in Ju *et al.*, 2013, while NS regulated in Woroniecka *et al.*, 2011.
Col5a1	collagen, type V, alpha 1	1.0 (8.24E-16)	1.4 (1.54E-31)	0.4 (0.01)	Upregulated in glomeruli in Woroniecka *et al.*, 2011 and Ju *et al.*, 2013.
Col5a3	collagen, type V, alpha 3	3.3 (2.74E-10)	5.2 (1.03E-25)	1.9 (0.0002)	NS regulated in glomeruli in Woroniecka *et al.*, 2011 and Ju *et al.*, 2013.
Col6a1	collagen, type VI, alpha 1	-0.3 (0.52)	2.0 (4.74E-08)	2.3 (8.54E-10)	Upregulated in glomeruli in Woroniecka *et al.*, 2011, while NS regulated in Ju *et al.*, 2013.

Col6a2	collagen, type VI, alpha 2	0.0 (0.97)	1.7 (8.35E-06)	1.7 (8.50E-05)	Upregulated in glomeruli in Woroniecka *et al.*, 2011 and Ju *et al.*, 2013.
Cxcl1	chemokine (C-X-C motif) ligand 1	1.4 (0.01)	3.1 (5.48E-10)	1.6 (0.01)	Upregulated in glomeruli in Ju *et al.*, 2013, while NS regulated in Woroniecka *et al.*, 2011.
Cxcl2	chemokine (C-X-C motif) ligand 2	1.3 (0.20)	3.4 (2.19E-05)	2.1 (0.04)	NS regulated in glomeruli in Woroniecka *et al.*, 2011 and Ju *et al.*, 2013.
Cyp2d9	cytochrome P450, family 2, subfamily d, polypeptide 9	1.9 (0.22)	1.3 (0.43)	-0.6 (0.86)	NA
Fn1	fibronectin 1	2.7 (1.58E-07)	4.2 (8.82E-19)	1.6 (0.01)	Upregulated in glomeruli in Woroniecka *et al.*, 2011 and Ju *et al.*, 2013.
Lox	lysyl oxidase	1.3 (0.0001)	3.2 (1.89E-29)	2.0 (2.39E-11)	Downregulated in glomeruli in Woroniecka *et al.*, 2011 and Ju *et al.*, 2013.
Mapk12	mitogen-activated protein kinase 12	-0.1 (0.51)	-0.5 (0.0002)	-0.4 (0.03)	NS regulated in glomeruli in Ju *et al.*, 2013.
Mmp12	matrix metallopeptidase 12	5.7 (3.78E-36)	6.3 (8.38E-46)	0.7 (0.08)	NS regulated in glomeruli in Woroniecka *et al.*, 2011 and Ju *et al.*, 2013.
Mmp14	matrix metallopeptidase 14 (membrane-inserted)	0.7 (1.74E-10)	0.8 (6.79E-15)	0.1 (0.59)	NS regulated in glomeruli in Woroniecka *et al.*, 2011, while downregulated in Ju et al., 2013.
Mmp3	matrix metallopeptidase 3	2.1 (1.96E-05)	2.2 (4.96E-06)	0.1 (0.96)	in glomeruli in Woroniecka *et al.*, 2011, while NS regulated in Ju *et al.*, 2013.
Mmp7	matrix metallopeptidase 7	3.6 (0.27)	6.4 (0.02)	2.8 (0.58)	Upregulated in glomeruli in Woroniecka *et al.*, 2011 and Ju *et al.*, 2013.
Mmp8	matrix metallopeptidase 8	3.7 (2.48E-06)	3.0 (0.0002)	-0.7 (0.69)	NS regulated in glomeruli in Woroniecka *et al.*, 2011.
Nphs1	nephrosis 1, nephrin	-0.3 (0.02)	-0.8 (3.99E-16)	-0.6 (1.86E-06)	Downregulated in glomeruli in Woroniecka *et al.*, 2011 and Ju *et al.*, 2013.
Nphs2	nephrosis 2, podocin	0.1 (0.40)	-0.4 (0.002)	-0.5 (7.09E-05)	Downregulated in glomeruli in Woroniecka *et al.*, 2011, while NS regulated in Ju *et al.*, 2013.
Rbp2	retinol binding protein 2, cellular	3.0 (0.24)	0.9 (0.73)	-2.1 (0.42)	NA
Serpine1	serine (or cysteine) peptidase inhibitor, clade E, member 1	0.6 (0.02)	2.1 (1.58E-26)	1.5 (2.38E-13)	NS regulated in glomeruli in Woroniecka *et al.*, 2011.
Timp1	tissue inhibitor of metalloproteinase 1	2.0 (0.0007)	3.0 (3.01E-08)	1.0 (0.26)	NS regulated in glomeruli in Woroniecka *et al.*, 2011, while upregulated in Ju *et al*., 2013.
Tlr4	toll-like receptor 4	0.6 (0.005)	0.7 (0.0002)	0.1 (0.75)	NS regulated in Ju *et al.,* 2013, but upregulated in Verzola *et al*., 2014.
Ugt1a10	UDP glycosyltransferase 1 family, polypeptide A10	1.4 (0.68)	2.8 (0.41)	1.3 (0.69)	NA
Vcam1	vascular cell adhesion molecule 1	-0.4 (0.08)	0.4 (0.04)	0.8 (0.0001)	Upregulated in glomeruli in Woroniecka *et al.*, 2011 and Ju *et al.*, 2013.